Lab on a Chip

PAPER

View Article Online
View Journal | View Issue

Cite this: *Lab Chip*, 2017, **17**, 3437

Image-based feedback and analysis system for digital microfluidics†

Philippe Q. N. Vo, [ab] Mathieu C. Husser, [bc] Fatemeh Ahmadi, [ab] Hugo Sinha [ab] and Steve C. C. Shih *[abc]

Received 4th August 2017,
Accepted 29th August 2017

DOI: 10.1039/c7lc00826k

rsc.li/loc

Digital microfluidics (DMF) is a technology that provides a means of manipulating nL–μL volumes of liquids on an array of electrodes. By applying an electric potential to an electrode, these discrete droplets can be controlled in parallel which can be transported, mixed, reacted, and analyzed. Typically, an automation system is interfaced with a DMF device that uses a standard set of basic instructions written by the user to execute droplet operations. Here, we present the first feedback method for DMF that relies on imaging techniques that will allow online detection of droplets without the need to reactivate all destination electrodes. Our system consists of integrating open-source electronics with a CMOS camera and a zoom lens for acquisition of the images that will be used to detect droplets on the device. We also created an algorithm that uses a Hough transform to detect a variety of droplet sizes and to detect singular droplet dispensing and movement failures on the device. As a first test, we applied this feedback system to test droplet movement for a variety of liquids used in cell-based assays and to optimize different feedback actuation schemes to improve droplet movement fidelity. We also applied our system to a colorimetric enzymatic assay to show that our system is capable of biological analysis. Overall, we believe that using our approach of integrating imaging and feedback for DMF can provide a platform for automating biological assays with analysis.

Introduction

Digital microfluidics (DMF) enables the manipulation of droplets on an electrode array surface by the application of electric potentials.[1,2] The DMF system has been known to provide a means of manipulating droplets for a wide range of volumes (pL–μL range) and each droplet can be transported, mixed, reacted, and analyzed. It has become a natural fit for integrating fluid handling for a vast range of applications requiring multiplexing, such as synthetic biology[3,4] and clinical diagnostics.[5,6] One of the main advantages with digital microfluidics is that it is highly amenable to integrating automation systems[7,8] and to external detectors (or internal in-line detectors[9,10]) for offline biological analysis.[11,12] Typically, an automation system is interfaced with a DMF device that accepts a standard set of basic instructions written by the user to execute droplet operations. For example, a user programs a set of instructions to dispense and to move droplets and to mix with other droplets for analysis. The ideal result is that every set of instructions would equate to a droplet operation (*e.g.*, mix, dispense, split). However, due to surface heterogeneity or the contents of the droplet, every application of a potential does not easily translate to a movement on the device. This behaviour is exacerbated when the droplet constituents contains cells or proteins as they tend to 'biofoul' the surface and render the device useless over a few actuations.[13,14]

One solution that can alleviate these problems is to use a control feedback system since they provide a means to 'sense' the droplet on the electrode.[15–19] By sensing the droplet on the electrode, a control algorithm can be executed to re-apply the potential at the destination electrode if the droplet is not present on that electrode. This can be repeated until the droplet completes the desired operation. Currently, the commonly used scheme for sensing droplets on DMF devices is to use capacitive sensing since the configuration of a DMF device can be electromechanically modeled with resistors and capacitors.[20] There have been a few papers in literature that are describing the integration of a capacitive feedback system with digital microfluidics. Ren *et al.*[15] and Gong and Kim[16] have used a ring oscillator circuit that uses frequency changes in the applied signal to monitor droplet dispensing. Shih *et al.*[17] have used a simple resistor and capacitor circuit

[a] *Department of Electrical and Computer Engineering, Concordia University, Montréal, Québec, Canada. E-mail: steve.shih@concordia.ca; Tel: +848 2424 x7579*
[b] *Centre for Applied Synthetic Biology, Concordia University, Montréal, Québec, Canada*
[c] *Department of Biology, Concordia University, Montréal, Québec, Canada*
† Electronic supplementary information (ESI) available. See DOI: 10.1039/c7lc00826k

to output voltage values which will be used to monitor droplet movement. And Gao *et al.*,[18] have implemented a fuzzy control algorithm that will compute optimized electrode charging time and real-time monitoring of the droplet on device. These methods use electronic circuits to sense and to monitor the droplet on device. However, a drawback with these methods is that these systems are not capable of detecting individual droplet failures. If a failure is detected, these systems require a re-application of a potential on the destination electrode for all the droplets on the device since it is not known which droplet on the device has failed in operation. This is not a favourable solution since excess activation of electrodes reduces the integrity of the dielectric and causes the surface to be prone to bio-fouling. Furthermore, these systems are only capable of sensing the droplet, but require external detectors (*e.g.*, well-plate readers)[21,22] for bioanalysis.

As an alternative to these different techniques, we present for the first time (to our knowledge) a feedback and analysis digital microfluidic system based on image-based techniques. There is a report of the use of droplet tracking software which tracks the droplet position, but does not provide feedback and analysis of the droplets on DMF devices.[23] In this paper, we describe our system which comprises of a camera with a focus zoom lens to monitor individual droplet movements and it enables the use for bioanalysis without requiring other detectors. We applied this system (1) to show multiplexed droplet dispensing and individual monitoring of droplet detection failure, (2) to actuate a range of fluids that are useful for biological assays, and (3) to validate that this image-based system can be used for analyzing an enzymatic assay using colorimetric pixel detection. Furthermore, we present the assembly and the operation details for the new system and believe that this system can be useful for scientists adopting DMF for their own biological applications.

Methods

Reagents and materials, device design, fabrication, and assembly, molecular cloning and protein expression are described in the ESI.†

Image-based automated feedback system

The feedback system and its setup is illustrated in Fig. 1. The digital microfluidic device is attached to a pogopin-control board with a 3D printed base platform (Fig. S1; STL file included in ESI†) that delivers electric potentials to the device for droplet movement. The pogopin board consists of a 2.5

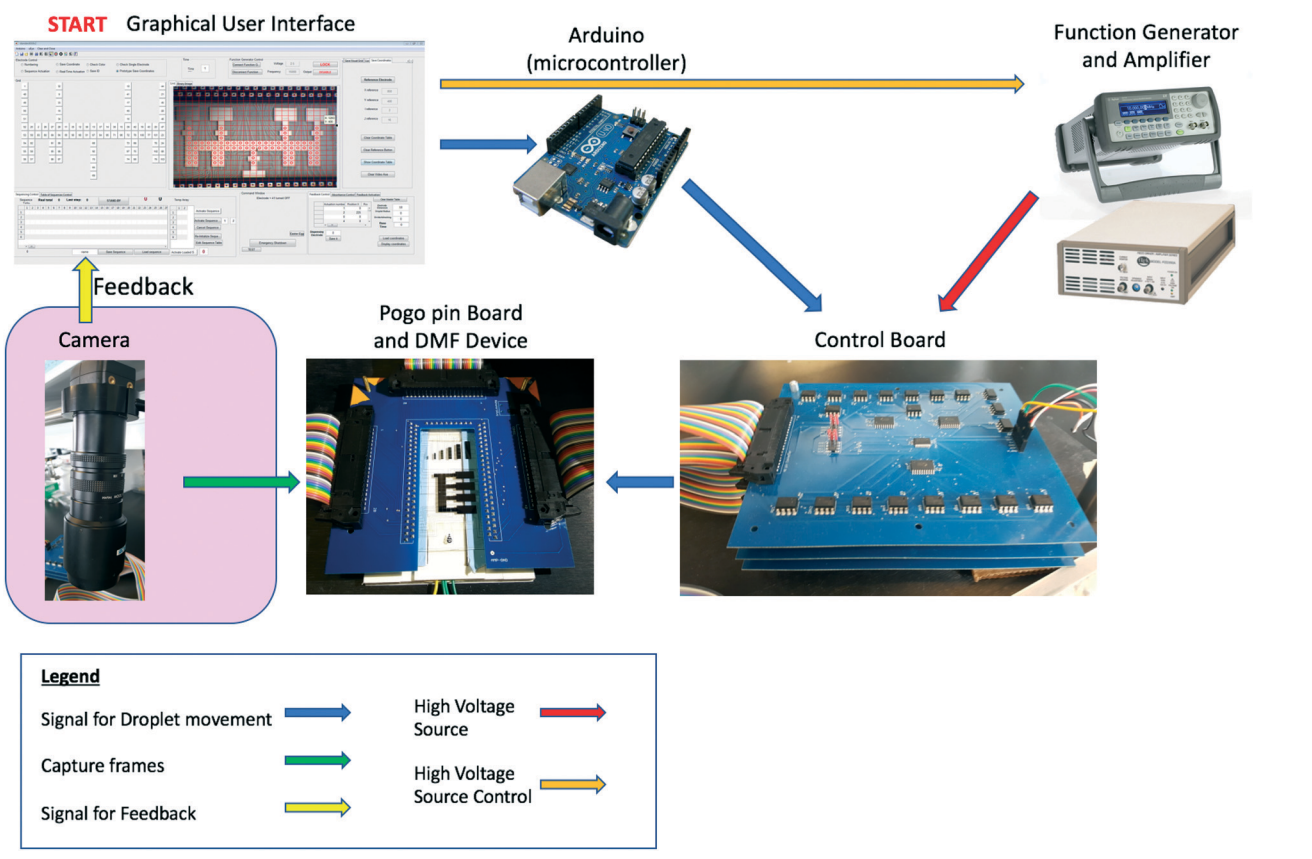

Fig. 1 Schematic of an image-based DMF feedback system. The feedback system consists of an Arduino, a function generator and amplifier, a switching control board, and a pogopin board with a 3D printed based to control the application of electric potentials that is applied to the device. The graphical user interface (GUI) is programmed by the user to deliver a series of droplet actuations and acquires images to manage the control logic for the sequential application of electric potentials.

mm thick board (printed by Gold Phoenix, Mississauga, ON) with surface mount pogo pins that will connect to the digital microfluidic device. These pogo pin boards are connected (*via* ribbon cable) to three control boards (printed by Gold Phoenix, Mississauga, ON) that house 80 solid state switches on each board. A typical output that connects to a pogopin is configured to designate two states: ground and high-voltage. Each switch is controlled by an I/O expander that is used to deliver 5 V power (*i.e.* logic high) to a switch *via* I^2C connection from the Arduino and an inverter that will automatically deliver a logic low (*i.e.* ground voltage) to a switch for the same output to prevent any short circuit between power and ground (see Fig. S2†). This connection scheme is repeated to allow 104 outputs on the digital microfluidic device. The Arduino Uno microcontroller and high-voltage amplifier (Trek Ltd., PZD700A) are connected to the control board and the function generator (Allied Electronics, 33210A Agilent) and is connected to the computer *via* USB connection. The main component of the feedback imaging system is a 3.0 MP CMOS Color USB camera (Edmund Optics, EO-3112C) attached to a 10× C-mount Close Focus Zoom lens (Edmund Optics, 54363). An additional lighting setup was configured around the camera and the device. This consisted of a Fiber Optic Illuminator 150 W (Edmund Optics, 38939) with a 23″ semi-rigid dual branch (Edmund Optics, 54212) that was directed onto a homemade backdrop. To acquire images, intensity of the fiber light was adjusted and the camera was rotated ~5° from the vertical center to enhance the outline of the droplet. High-resolution images (2048 × 1536 pixels) were acquired and used for droplet analysis and detection. All the electrical components are displayed in a BOM table provided in the ESI.†

Feedback software setup

The Arduino is controlled by an in-house made software using MATLAB (incl. in ESI†) which requires the image acquisition and processing, computer vision, an instrument control, and Arduino support toolboxes for execution. The files are included in the ESI† (*img_feedback.zip* file) with a video on how to setup and to execute the software. Briefly, to enable the feedback system, this requires configuring three parts of the software: (1) DMF grid configuration, (2) sequence generation, and (3) feedback and analysis setup. In DMF grid configuration, users can create their own designs that match their device design by entering a grid specifying the number of rows and columns and selecting the squares on the grid to match the user device design. Next, the user will input the 'electrode number' matching to the connection on the pogopin board and switch. The resulting DMF design grid can be saved for future use. In sequence generation, users have the capability to enable real-time control (*i.e.* on-demand actuation) or sequence-activated control (*i.e.* users create their own sequences). For real-time control, users can click on the electrode to enable real-time application of the electric potential to the electrode. For sequence-activated control, users can create a sequence by clicking on the electrode button and save the selection by enabling the 'space' key. This can be repeated, saved for future use, and activated when the user is ready for actuation. For either actuation method, users will enter values for voltage, time, and frequency which are parameters required to actuate the droplets on the device. In the feedback and analysis setup, a variety of parameters are required to enable the feedback system (see ESI† video). Briefly, users will create a visual grid that is used for storing the coordinates of the electrodes. Users will enter values for electrode size (in pixels), radius size (*i.e.* typically half of electrode size), detection box (*i.e.* region of detection), base time (*i.e.* time duration for one pulse), correction time (*i.e.* time duration for one correction), base voltage (*i.e.* initial voltage applied to the electrode), and jolt voltage (*i.e.* incremental voltage). Using this system, images were acquired and analyzed to check if the droplet is on the destination electrode. In addition, we created a program that will acquire images of the droplets that will automatically calculate the pixelated RGB channel values for biological analysis.

Droplet dispensing and movement

In conventional operation (without feedback), droplet dispensing was initiated by the application of an electric potential (~150 V_{RMS}; 10 kHz) to a reservoir electrode; then iteratively applied to three adjacent electrodes to stretch out the liquid from the reservoir. To 'dispense' the droplet, potentials were simultaneously applied to both the reservoir and the third adjacent electrode. Similarly, droplet movement was initiated by applying potentials to a desired electrode and iteratively applied to adjacent electrodes. This enabled the user to program the number of droplet movements (N_D) and record the number of successful droplet movements. To evaluate the feedback system, we tested four actuation schemes to determine the fidelity of droplet manipulation: (1) normal, (2) jolt, (3) correction, and (4) jolt and correction (Fig. S3a†). In the normal scheme, a re-application of the reference potential is applied to the destination electrode Y if there is a failure in droplet movement. In the jolt scheme, the destination electrode (Y) was re-actuated with a higher potential in increments set by the user (*i.e.* jolt voltage) during the setup of the feedback system. If droplet movement does not proceed to Y, this process is repeated until the voltage reaches a limit of 250 V_{RMS}. In the correction scheme, two electrodes – the source (X) and destination (Y) – are actuated with the same applied voltage. If there is a droplet movement failure, the scheme will (1) actuate both X and Y electrodes for a user-specified duration (*i.e.* the correction time) and (2) turn off electrode X, while leaving electrode Y on for an additional correction time. In the jolt and correction combination scheme, the program will start with the correction scheme and increase the voltage on electrode Y (by the jolt voltage) at the end of the correction scheme. For these schemes, the droplet velocities were measured for each movement, which is the ratio between the size of an electrode (D) and the base

time set by the user of one pulse (T_D) (*i.e.* $V = D/T_D$). In feedback mode, dispensing and movement followed a similar process with an additional time used for analyzing the images (T_I). The time for checking the images were typically ~500 ms. Hence, the droplet velocities were calculated as $V = D \times N_D/(N_A \times (T_I + T_D))$ where N_A is the number of electrode actuations. All experiments were conducted with device 1 (Table S1†) with a gap height of 70 μm.

β-Glucosidase enzymatic assay

The assay on-chip consisted of three different solutions loaded onto the DMF device reservoirs. First, a unit droplet of cell lysate was dispensed and actuated to each of the four assay mixing areas (see Table S1† for DMF design) using a starting voltage of 230 V_{RMS} at 15 kHz. The lysate was prepared from a colony of BL21(DE3) transformed with a plasmid containing BGL (β-glucosidase) gene (see Fig. S4 and S5† for plasmid map and sequence respectively) that was grown at 37 °C and induced at 0.4 O.D (~1.75 h starting at 0.1 O.D). The assay started by the addition of a droplet containing substrate to a droplet of cell lysate. The substrate solution contained 50 mM sodium-citrate at pH 7.0 and 4 mM 4-nitrophenyl β-D-glucopyranoside. The reactions were incubated at different times (0, 40, 80, and 120 min) and arrested by the addition of a unit droplet of 0.3 M glycine–NaOH on the assay areas on the device. Solutions contained 0.05% final concentration of F-68 Pluronics. Three replicate trials using three different devices with gap heights of 280 μm were conducted with feedback control. The blue color channel pixel intensity of the droplet was acquired using the imaging-feedback system after addition of the glycine–NaOH droplet and plotted over time.

Results and discussion

Image-based feedback system

A custom MATLAB program (Mathworks, Natick, MA) was written to implement the new imaging and analysis feedback system; this program is freely available in the ESI.† To setup the feedback system, a reference image was acquired with no visible droplets on the electrode path except on the reservoirs. This reference image is acquired for edge detection of the droplet and subtraction techniques for droplet detection (a method similarly used in these studies[23] and[24]). To detect the droplet position, four operations were executed every 500 ms to determine if the droplet dispensed from the reservoir or moved successfully onto the destination electrode (Fig. 2). The destination electrode is any electrode (*i.e.* a reservoir or actuation electrode) that has an applied potential. Operation (1) acquires a capture frame that shows the droplet on the source (shown as 'x') and the destination (shown as 'y')

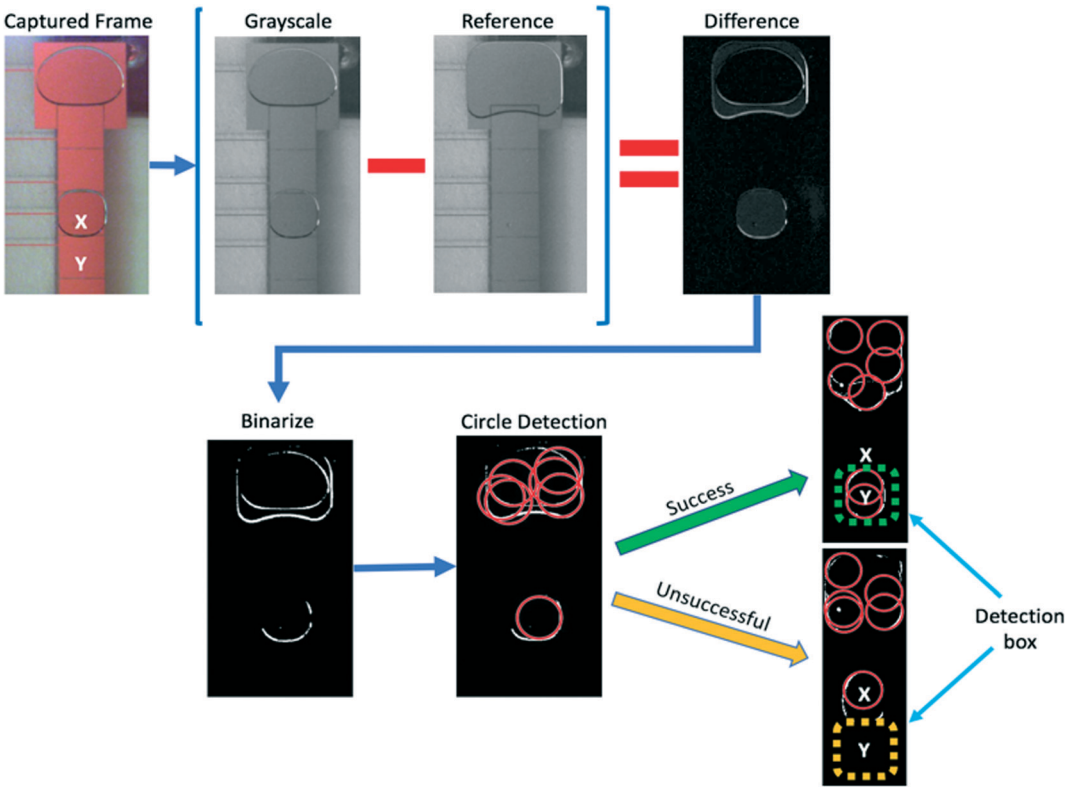

Fig. 2 Algorithm of the image-based feedback system. A droplet is resting on the x electrode and the automation system applies potential to the y electrode. A frame is captured after an actuation. A difference frame is created by taking the difference from a grayscale image and a reference image (*i.e.* no dispensed droplets). A binarized frame is created from the difference frame. From this frame, a Hough transform allows the detection of circles and returns a successful or unsuccessful result depending on the location of the actuated droplet and the user-defined detection box.

electrode. Operation (2) calculates a difference image by subtracting a reference image (taken from setup) from a gray-scale image such that it identifies the droplet boundary. Operation (3) binarizes the difference image (*i.e.* digitizing the image to 1's and 0's) which is to intensify the faint droplet boundaries to stronger ones similar to intensity thresholding or maximum computation.[25,26] Operation (4) uses a Hough transform[27–29] to detect the circles (*i.e.* shape of droplet) at the destination electrode and returns a successful or unsuccessful result. An unsuccessful droplet movement would enable the program to start one of the four actuation schemes (described in methods) to the destination electrode 'y', while a successful droplet movement continues to the next droplet movement event in the sequence. Since we actuate simultaneously two electrodes (reservoir and the third adjacent electrode) for dispensing, we only consider the actuation electrode (not the reservoir) for detecting dispensed droplets. A control logic flowchart showing the feedback and analysis steps is presented Fig. S6.†

Characterization of the feedback system

In initial experiments, we observed that the droplet detection efficacy using our imaging software was not uniform on different regions on the device (*i.e.* ~40% droplets were detected). We hypothesize that this could be due to the lighting from the environment and the alignment of the camera with respect to the device, which can induce false positive or negatives. To mitigate this, we designed an external backdrop (Fig. 3A) that will maintain uniform lighting around the device. This external backdrop consists of a white-coloured box with a dual-branch fiber optic illuminator to guide the light into the box. After this modification, we characterized the lighting system by examining the lighting intensity and the alignment of the camera and determining its effect on droplet detection using our detection software (Fig. 3B). In these experiments, we collected a series of test images containing a droplet at a reference electrode and moving it to an adjacent electrode. Based on our results, no errors in droplet detection were observed at the angles and light intensities tested, demonstrating the efficacy of our imaging algorithm. Although we obtained high success of detection, we chose a camera angle of 5° since we obtained optimal contrast between the droplet and the electrodes on the device.

Next, we performed experiments to assess the impact of the radius size parameter and the size of the electrode on droplet detection. Here, we used device #1 (Table S1†) containing different sized electrodes and systematically changed the box size of detection to determine if the droplet can be detected by our imaging feedback system. We used electrode sizes of 1, 1.5, 2, 2.5, and 3 mm that hold liquid volumes of 70, 157.5, 280, 437.5, and 630 nL (for a 70 μm spacer) respectively covering the area of the electrode. For each electrode size, we systematically changed the size of the detection box (in pixels) and then executed the image detection software to determine if the droplet is successfully

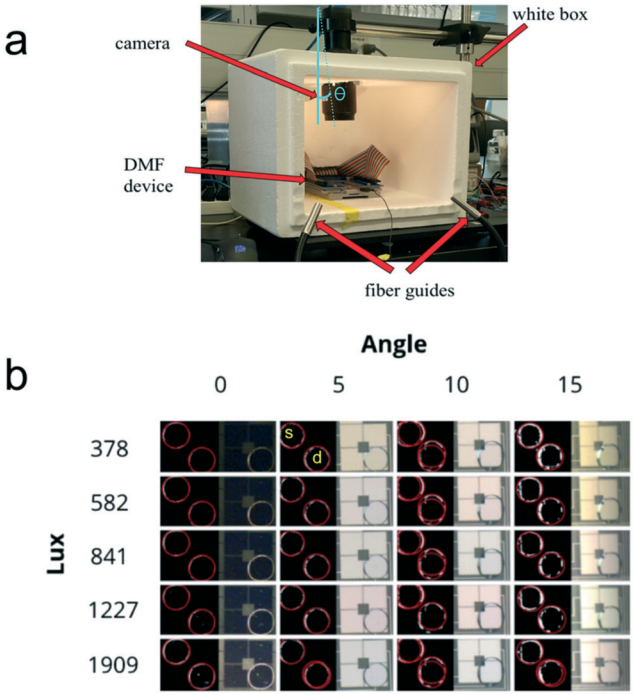

Fig. 3 Effect of light intensity and alignment of camera on droplet detection. (a) Setup of the camera shown with the measured angle surrounded with a white backdrop. (b) A set of images showing the success of droplet detection as a function of camera angle (°) at different light intensities (lux). A droplet was placed at a source electrode (labelled as s) and were actuated to a destination electrode (labelled as d) to determine if the image software can detect the droplet. Two images (circle detection – left and original – right) were shown for each angle and light intensity.

detected. This is an important feature in the program to ensure a range of droplet volumes can be detected, especially in cases where droplets are merged together. As shown in Fig. 4,

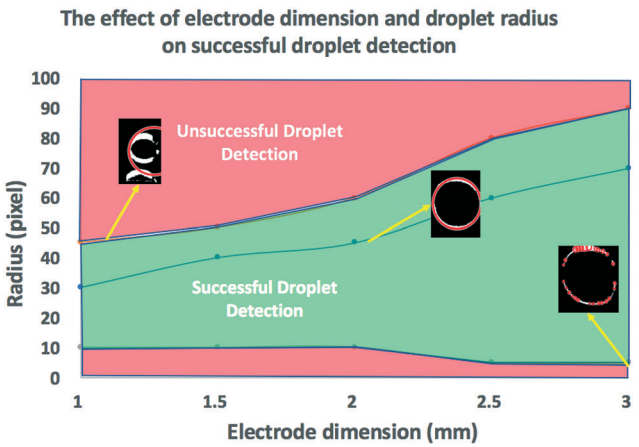

Fig. 4 The effect of electrode dimension and droplet radius on droplet detection. A smaller electrode dimension (1 mm) has a smaller range of successful droplet detection compared to a larger electrode dimension (3 mm). Insets in the graph show image views of a successful droplet detection. The middle line is showing the case when a radius that is half of the electrode size is used.

a smaller electrode dimension (*e.g.*, 1 mm) has a smaller range for successful droplet detection compared to a larger electrode dimension (*e.g.*, 3 mm). False positives (*i.e.* droplets are 'detected' when there is not droplet present) or negatives (*i.e.* droplets are present and not detected) can be avoided if the detection box size is chosen within the upper and lower limits (*i.e.* shown in the coloured green region). The ideal detection box size is one-half of the electrode size since we obtain 100% successful droplet detection.

After sensing the droplet position, we initially programmed our feedback system to repeat the application of an electric potential onto the destination electrode. However, we observed frequent failures after detection using this typical scheme especially for liquids that have proteins (~10% of the 50 programmed movements were successful). Therefore, this enabled us to assess different actuation schemes by calculating the number of completed droplet movement steps and the number of feedback actuations required after a failure is encountered. Some groups have introduced upgraded hardware solutions,[30,31] where some have introduced the elevation of the electrode-driving voltage[32,33] to improve droplet movement. Here, we assessed multiple actuation schemes that can be used to move droplets that resist movement. We tested three different schemes: jolt, correction, and jolt and correction (as described in the methods) and compared it to the normal scheme (*i.e.* reapplication of the potential of same magnitude) using complete cell media consisting of RPMI 1640 with 10% FBS. We did not test other types of liquids since feedback-sensing is typically not required for liquids without proteins as per our observation (see next section) and shown from other studies.[17,18] In Table 1, the jolt scheme temporarily increased the electric potential by 10 V_{RMS} each cycle and is successful in moving the droplet ~16% of the time. However, this actuation scheme frequently would compromise the dielectric causing electrolysis at high voltages which renders the device useless. Furthermore, the increase in electric potential induced droplets to move to the destination electrode but frequently would 'pull back' to the source electrode after applying the increased voltage on the destination electrode (Fig. S3b†). We hypothesized that a different switching scheme may alleviate this 'pull-back' problem – specifically, turning on both the source and the destination electrode will enable overlap with the destination electrode while preventing any 'pull-back' of the droplet to the source. Our data validated our hypothesis – we observe an significant increase in successful droplet movement after the correction actuation scheme is initiated compared to the jolt scheme – 16% *vs.* 100%. In most cases when the initial droplet movement has failed, generally only one correction actuation was required while two jolt actuations were required per failed droplet movement due to the pull-back problem. For completion, we tested the combination of the jolt and correction and observed similar success completion rates (100%) as to using only the correction scheme. On average, only one jolt and correction actuation were typically required since the jolt was used in combination with the correction. This suggested that the correction scheme with feedback is most favorable for moving liquids that is similar in viscosity to complete cell media on DMF devices since it prevents the 'pull-back' problem and avoids any degradation to the dielectric.

Droplet dispensing and movement

Droplet dispensing is an operation commonly conducted on digital microfluidic devices. Dispensing is defined as a success if the dispensing protocol produced a unit droplet with user specified volume. Several studies have examined the droplet dispensing and have characterized the mechanism of droplet dispensing.[15,16,34] These groups investigate the variation in volume of dispensed droplets and correct the variation of the volume by capacitive sensing and feedback control.[15,16] Unfortunately, these systems mainly focused on repetitive dispensing of droplets from a reservoir – *i.e.* serially dispensing one droplet during a sequence – and studying variation in the volume of dispensed droplets. A drawback with their systems is that they are not capable of detecting individual dispensing failures, only detecting if there is a variation in volume present. To fully harness the advantage of digital microfluidics is to be able multiplex dispensing during one sequence – *i.e.* parallel dispensing of droplets. We hypothesized that application of the imaging feedback control to multiplexed dispensing would enable detection of individual dispensing failures. As shown in Fig. 5, three droplets containing water and one droplet containing LB media were dispensed in parallel following the typical actuation procedure for dispensing (described in methods). In rows 2–4, dispensing was a success as droplets were observed within the detection box (*i.e.* destination electrode) while in row 1, dispensing failed and required sensing and feedback to complete the droplet dispensing process. Three replicate trials were conducted and each trial showed the droplet dispensing protocol regularly failing to produce a unit droplet with an initial application of electric potential for viscous liquids, especially for liquids containing proteins (*e.g.*, LB media). This suggests that there is a need for sensing and feedback for

Table 1 Comparison of different feedback actuation schemes

Actuation schemes	Completed actuations out of 50	Total no. of feedback actuations per 50 steps	Average feedback actuation per step
Control	4.7 ± 1.8	17	4
Jolt	8 ± 2.8	16	2
Correction	50	8.1	0.162 ≈ 1
Jolt + correction	50	3.6	0.072 ≈ 1

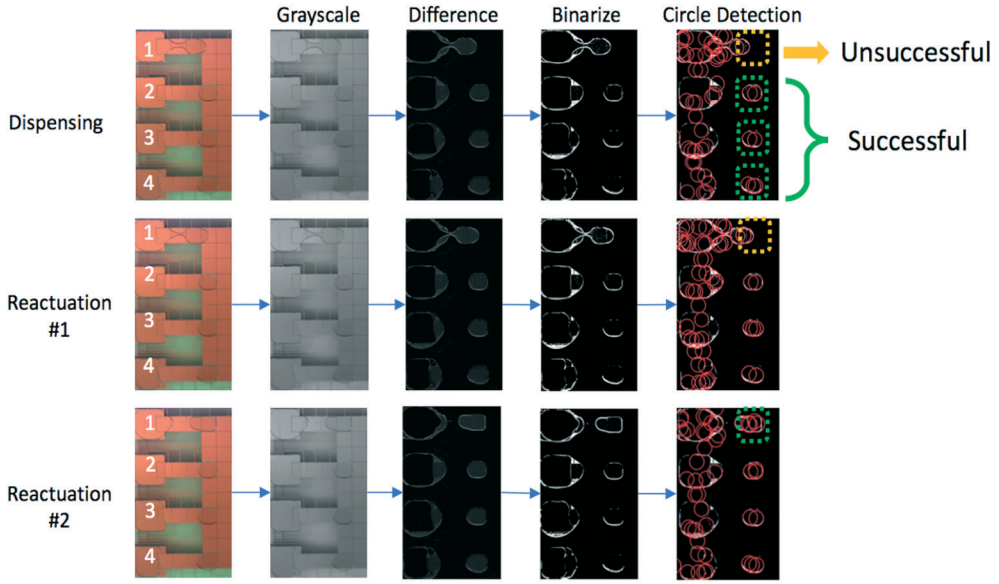

Fig. 5 Multiplexed dispensing showing detection of a single droplet dispensing failure. Row 1 to 4 are dispensed simultaneously. Rows 2–4 show dispensing success while a failure in row 1 is observed. Two additional applications of potentials (#1 and #2) are only applied to row 1 while droplet on rows 2–4 continue with the program sequence.

dispensing liquids containing proteins. Individual detection of dispensed droplets becomes important for biological assays (see next section) as it reapplies electric potentials to only failed droplet movements without excess application to electrodes with successful droplet movements. This will minimize biofouling since more actuations reduces the contact angle of the droplet.[13] Furthermore, excess actuations will increase degradation of the dielectric layer which reduces the lifetime of the device.[32]

In addition to droplet dispensing, we also validated our image-based feedback system by evaluating droplet movement for four liquids that are commonly used in biological assays: DI water, PBS, LB media with *E. coli* (at O.D. 1.5), and RPMI with 10% FBS. In our tests, droplets were actuated across a linear device consisting of 10 electrodes and were repeated five times giving rise to a total of 50 movements. We systematically changed actuation base times (T_D – 100, 500, 1000, 1500 ms) and measured the number of successful droplet movements out of 50 steps. As shown in Fig. 6, the number of successful movements is highly dependent on T_D. Specifically, with a single application of an electric potential with no feedback, higher velocities (or fast base times: 100 or 500 ms) generally results in poor droplet movement for non-water liquids. Furthermore, there is high variability of success for liquids that contain proteins (*e.g.*, RPMI with 10% FBS and LB media with *E. coli*) at slower velocities (1.65 mm s^{-1} and 2.48 mm s^{-1}) due to the heterogeneous mixture of the solution. This is problematic for digital microfluidics as the droplet transportation efficiency is highly variable for protein-rich liquids at low velocities ($\leq$5 mm s^{-1}) and therefore depends on chance for completion. However, with our image-based feedback system we observe improvements in velocities (*i.e.* faster for the droplet to reach the destination) and more importantly an increase in the number of successful droplet movements. In Table 2, we obtained perfect droplet movement fidelity (out of 50 movements) with average velocities of ~2.5 mm s^{-1} and 2–3× increase in velocities (compared to no feedback) for protein-rich liquids. In addition, fast base times of 100 ms are favourable for moving droplets containing no proteins (*e.g.*, PBS and H_2O) while 500 ms are favourable for protein-rich liquids (*e.g.* RPMI with FBS and LB media). This is a similar observation compared to a previous study where the fast base times are not enough to account for the viscosity of the liquid and slow base times

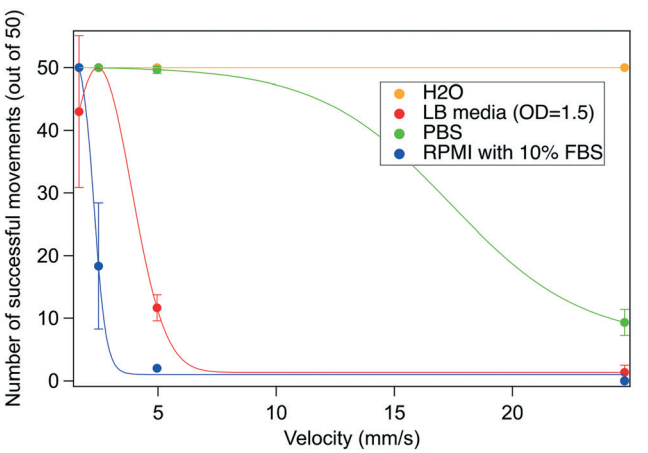

Fig. 6 The effect of droplet movement on DMF devices without feedback. Four liquids: DI water, PBS, RPMI with 10% FBS (complete cell media), and LB media (with O.D = 1.5) were tested on 10 electrodes at different velocities (*i.e.* different base times – T_D – 100, 500, 1000, 1500 ms) and were repeated five times to give a total of 50 actuations. The error bars are ± one standard deviation from three replicate trials.

Table 2 Velocities of liquids with feedback

Liquids	No. of successful movements	Base time (ms)	Avg. total time (s)	Avg. velocity (mm s^{-1})
Water	**50**	**100**	**6.10**	**18.66**
	50	500	26.30	4.28
	50	1000	53.83	2.11
	50	1500	78.77	1.43
PBS	**50**	**100**	**48.31**	**2.71**
	50	500	50.08	2.47
	50	1000	74.04	1.67
	50	1500	99.83	1.24
RPMI	50	100	73.61	1.69
	50	**500**	**51.50**	**2.41**
	50	1000	80.39	1.54
	50	1500	134.60	0.95
LB	50	100	64.06	1.93
	50	**500**	**49.18**	**2.52**
	50	1000	74.31	1.67
	50	1500	101.30	1.22

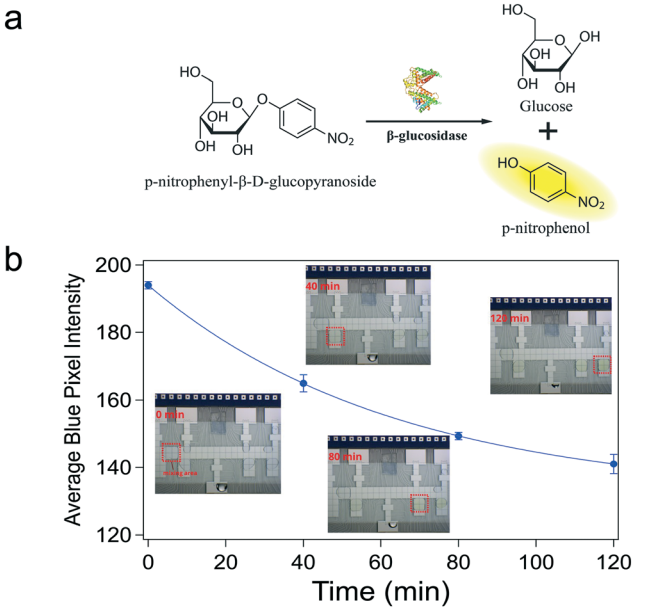

Fig. 7 β-Glucosidase enzymatic assay using the imaging feedback system. (a) Chemical scheme of the enzymatic assay. (b) A curve depicting the average blue channel pixel intensity as a function of time. The average blue channel pixel intensity was collected every 40 min intervals on device #2 with our image-based feedback system. Inset shows series of frames at the different time intervals depicting the enzyme assay and where the droplets were analyzed (red box). Each experiment was repeated in triplicate on separate devices, and error bars are ± 1 SD.

are exacerbating surface fouling.[17,18] Therefore, this clearly shows that there is a need for an image-based feedback system for moving protein-rich liquids that will automatically optimize the base times to move these types of liquids.

β-Glucosidase enzymatic assay

To demonstrate the applicability of our image-based feedback system, we examined the activity of a β-glucosidase enzyme that is useful for the production of biofuels. Cellulose has great potential as a renewable energy source and the enzymatic hydrolysis which is completed by β-glucosidases is a promising green alternative for the production of fuels.[35] The typical model for analyzing kinetics of a β-glucosidase enzyme is to use a chromogenic model substrate *para*-nitrophenyl-β-glucoside (pNPG) that will produce glucose and *para*-nitrophenol upon hydrolysis (Fig. 7a). The liberation of *para*-nitrophenol (pNP) gives a yellow color product which we hypothesize can be monitored by our image-based feedback system.

Some groups have incorporated image processing techniques on droplets by capturing an image and use it either as a threshold value for intensity or comparing the image captured from a video with a standard image.[28,36–38] For our kinetics analysis, we used a different approach[39] to measure the activity of the enzyme. Using device #2 (Table S1†), we used the automated feedback system to dispense and to move the substrate and lysate to the mixing and detection areas on the device and calculated the RGB profile for a region of interest (ROI) inside the droplet without any external optical detectors (*e.g.*, well-plate reader or optical fibers) at different time intervals (Fig. 7b). Using our MATLAB program *colour_analysis.m* (in *colour_assay.zip*), we selected a ROI that is covering 25% of the droplet and averaged the pixel intensities for each colour channel: red, green, and blue. As expected, the red and green channels did not show any significant difference in the pixel analysis of the pNP yellow product (data not shown). From the blue channel, as shown in Fig. 7b, the graph depicts the change in yellow color as a function of time showing differences in blue channel pixel intensities for the pNP product in reaction droplets that were mixed with feedback control. In initial experiments without feedback, moving and dispensing droplets containing the lysate and the substrate were difficult due to large gap heights (~280 μm) which caused the experiment to fail over 95% of the time. However, with our feedback system, we are able to dispense droplets with >99% success rate while moving droplets to the destination electrode with perfect fidelity. Additionally, we are able to merge the droplets and to detect this droplet with the same fidelity. This high success rate is due to the capability of the feedback system to correct individual droplet operation failures while concurrently actuating droplets that were successful in movement to the destination. Using our image-based feedback approach allowed for moving and dispensing protein-rich liquids and analyzing the product of an enzymatic assay.

In the same experiments, we were also able to extract first order rate constants and compared it to off-chip reactions. The extracted value generated from our image-based feedback system is k_{DMF} = 0.167 h^{-1} and the rate constant from off-chip experiments is k_{PLATE} = 0.504 h^{-1} (Fig. S7†). We note that there are some differences in the rate constants since we are using different pieces of optical equipment (camera *vs.* well-plate reader) to analyze the pNP product. In the future,

we propose that integration of lenses and filters to our camera setup can give a closer estimate to the well-plate reaction rate constant. Nevertheless, we propose that discovering relative activities between enzymes or any applications requiring automated mixing of protein-rich liquids will be highly suitable for our image-based feedback system.

Conclusion

We have demonstrated an automated image-based feedback system to move and to dispense biological fluids on digital microfluidic devices. The image-based feedback system uses a reference and subtracting technique with a Hough transform to visualize the droplets on the device. We characterized the image-based feedback system and determined the optimal camera angle, lighting intensity, radius of detection, and correction method to implement for high success of droplet detection. Furthermore, this system is capable of detecting individual droplet dispensing and movement failures and implementing feedback while concurrently continuing with other droplet operations on the device. To show the utility of our system, we applied it to conducting an enzymatic assay that uses the image-based algorithm to analyze the enzymatic product without requiring any other external detectors. Our image-based feedback and analysis system is an automated solution for multiplexed biological assays whose performance exceeds either normally operated digital microfluidic devices or previous reported feedback systems.

Conflicts of interest

There are no conflicts to declare.

Acknowledgements

We thank Abtin Ghodoussi, Kaleem Corbin, and Minghong (Meko) Deng for their initial work with the automation control system. We also thank the Natural Sciences and Engineering Research Council (NSERC), the Fonds de recherché Nature et technologies (FRQNT), and the Canadian Foundation of Innovation (CFI) for funding. P. Q. N. V. thanks NSERC and M. C. H. thanks Concordia University for an undergraduate scholarship (USRA), and F. A. and H. S. thanks Concordia University for FRS funding.

References

1 K. Choi, A. H. Ng, R. Fobel and A. R. Wheeler, *Annu. Rev. Anal. Chem.*, 2012, **5**, 413–440.
2 E. Samiei, M. Tabrizian and M. Hoorfar, *Lab Chip*, 2016, **16**, 2376–2396.
3 P. C. Gach, S. C. Shih, J. Sustarich, J. D. Keasling, N. J. Hillson, P. D. Adams and A. K. Singh, *ACS Synth. Biol.*, 2016, **5**, 426–433.
4 S. C. C. Shih, G. Goyal, P. W. Kim, N. Koutsoubelis, J. D. Keasling, P. D. Adams, N. J. Hillson and A. K. Singh, *ACS Synth. Biol.*, 2015, **10**, 1151–1164.
5 S. Kalsi, M. Valiadi, M. N. Tsaloglou, L. Parry-Jones, A. Jacobs, R. Watson, C. Turner, R. Amos, B. Hadwen, J. Buse, C. Brown, M. Sutton and H. Morgan, *Lab Chip*, 2015, **15**, 3065–3075.
6 A. H. Ng, M. Lee, K. Choi, A. T. Fischer, J. M. Robinson and A. R. Wheeler, *Clin. Chem.*, 2015, **61**, 420–429.
7 M. D. M. Dryden, R. Fobel, C. Fobel and A. R. Wheeler, *Anal. Chem.*, 2017, **89**, 4330–4338.
8 S. C. C. Shih, I. Barbulovic-Nad, X. Yang, R. Fobel and A. R. Wheeler, *Biosens. Bioelectron.*, 2013, **42**, 314–320.
9 X. Zeng, K. Zhang, J. Pan, G. Chen, A. Q. Liu, S. K. Fan and J. Zhou, *Lab Chip*, 2013, **13**, 2714–2720.
10 L. Lin, R. D. Evans, N. M. Jokerst and R. B. Fair, *IEEE Sens. J.*, 2008, **8**, 628–635.
11 L. Malic, T. Veres and M. Tabrizian, *Lab Chip*, 2009, **9**, 473–475.
12 S. H. Au, S. C. C. Shih and A. R. Wheeler, *Biomed. Microdevices*, 2011, **13**, 41–50.
13 S. H. Au, P. Kumar and A. R. Wheeler, *Langmuir*, 2011, **27**, 8586–8594.
14 S. L. Freire and B. Tanner, *Langmuir*, 2013, **29**, 9024–9030.
15 H. Ren, R. B. Fair and M. G. Pollack, *Sens. Actuators, B*, 2004, 319–327.
16 J. Gong and C. J. Kim, *Lab Chip*, 2008, **8**, 898–906.
17 S. C. C. Shih, R. Fobel, P. Kumar and A. R. Wheeler, *Lab Chip*, 2011, **11**, 535–540.
18 J. Gao, X. Liu, T. Chen, P. I. Mak, Y. Du, M. I. Vai, B. Lin and R. P. Martins, *Lab Chip*, 2013, **13**, 443–451.
19 S. Sadeghi, H. Ding, G. J. Shah, S. Chen, P. Y. Keng, C. J. Kim and R. M. van Dam, *Anal. Chem.*, 2012, **84**, 1915–1923.
20 D. Chatterjee, H. Shepherd and R. L. Garrell, *Lab Chip*, 2009, **9**, 1219–1229.
21 A. H. Ng, B. B. Li, M. D. Chamberlain and A. R. Wheeler, *Annu. Rev. Biomed. Eng.*, 2015, **17**, 91–112.
22 I. Barbulovic-Nad, S. H. Au and A. R. Wheeler, *Lab Chip*, 2010, **10**, 1536–1542.
23 A. S. Basu, *Lab Chip*, 2013, **13**, 1892–1901.
24 M. A. Alyassin, S. Moon, H. O. Keles, F. Manzur, R. L. Lin, E. Haeggstrom, D. R. Kuritzkes and U. Demirci, *Lab Chip*, 2009, **9**, 3364–3369.
25 J. Canny, *IEEE Trans. Pattern Anal. Mach. Intell.*, 1986, **8**, 679–698.
26 D. Ziou and S. Tabbone, *Int. J. Pattern Recognit. Image Anal.*, 1998, **8**, 537–559.
27 M. Smereka and I. Dul, *Int. J. Appl. Math. Comput. Sci.*, 2008, **18**, 85–91.
28 M. Girault, H. Kim, H. Arakawa, K. Matsuura, M. Odaka, A. Hattori, H. Terazono and K. Yasuda, *Sci. Rep.*, 2017, **7**, 40072.
29 H. N. Joensson, M. Uhlen and H. A. Svahn, *Lab Chip*, 2011, **11**, 1305–1310.
30 N. Rajabi and A. Dolatabadi, *Colloids Surf., A*, 2010, **365**, 230–236.
31 D. Brassard, L. Malic, F. Normandin, M. Tabrizian and T. Veres, *Lab Chip*, 2008, **8**, 1342–1349.
32 C. Dong, T. Chen, J. Gao, Y. Jia, P. I. Mak, M. I. Vai and R. P. Martins, *Microfluid. Nanofluid.*, 2015, **18**, 673–683.

33 T. Chen, C. Dong, J. Gao, Y. Jia, P. I. Mak, M. I. Vai and R. P. Martins, *AIP Adv.*, 2014, **4**, 047129.
34 K. S. Elvira, R. Leatherbarrow, J. Edel and A. Demello, *Biomicrofluidics*, 2012, **6**, 22003–2200310.
35 H. Teugjas and P. Valjamae, *Biotechnol. Biofuels*, 2013, **6**, 105.
36 H. Kim, H. Terazono, Y. Nakamura, K. Sakai, A. Hattori, M. Odaka, M. Girault, T. Arao, K. Nishio, Y. Miyagi and K. Yasuda, *PLoS One*, 2014, **9**, e104372.
37 E. Zang, S. Brandes, M. Tovar, K. Martin, F. Mech, P. Horbert, T. Henkel, M. T. Figge and M. Roth, *Lab Chip*, 2013, **13**, 3707–3713.
38 A. M. Esmaeel, A. B. Sharkawy, T. ElMelegy and M. Abdelgawad, *18th International Conference on Miniaturized Systems for Chemistry and Life Sciences*, San Antonio, TX, USA, 2014, pp. 2339–2341.
39 P. A. Wijethunga, Y. S. Nanayakkara, P. Kunchala, D. W. Armstrong and H. Moon, *Anal. Chem.*, 2011, **83**, 1658–1664.

